Measurements Made in the SPS with a Rest Gas Profile Monitor by Collecting Electrons

C. Fischer, J. Koopman

European Organisation for Nuclear Research (CERN)
CH-1211 Geneva 23, Switzerland

Abstract. Measurements have regularly been performed during the 1999 run, using the Rest Gas Monitor installed in the SPS. The exploited signal resulted from electrons produced by ionisation of the rest gas during the circulating beam passage. A magnetic field parallel to the electric extraction field was applied to channel the electrons. Proton beam horizontal transverse distributions were recorded during entire SPS acceleration cycles, between 14 GeV/c and 450 GeV/c and for different beam structures and bunch intensities. The influence of several parameters on the measured beam profiles was investigated. Results are presented and analysed in order to determine the performance that can be expected.

INTRODUCTION

A modified rest gas monitor measuring horizontal transverse beam distributions was installed and tested in the SPS throughout 1999. The goal was to determine the ability of such a monitor to analyse beams having transverse distributions of one millimeter (rms) or less. This will be needed in the SPS and in the LHC, below 2 TeV, until a monitor using synchrotron radiation can take over [1]. In order to improve the precision usually obtained with rest gas monitors when ions are collected, the signal from electrons is exploited. The electron transverse excursion at the collecting plate, due to their initial velocity and the proton beam induced space charge forces, is reduced by channelling them along magnetic field lines, parallel to the extracting electric field. This method is already in use for larger beam dimensions [2]. A monitor provided by DESY [3] was incorporated, after having been modified, within a magnet, the gap of which was increased from 220 mm to 700 mm. The obtained field at full power is B = 0.06 T in the active area of the monitor. The corresponding set-up was already described in [4] and preliminary results reported. The present paper deals with the experience gained and with the analysis of the data collected over the past year.

HARDWARE DESCRIPTION

Electrons, liberated from the ionised gas, are collected, by means of the applied electric and magnetic fields, onto a Micro Channel Plate (MCP), a Hamamatsu F2805-03. When leaving the MCP, they are accelerated onto a Proxitronic P46 ($Y_3Al_5O_{12}$:CE) phosphor screen, with an Indium Tin Oxide (ITO) layer.

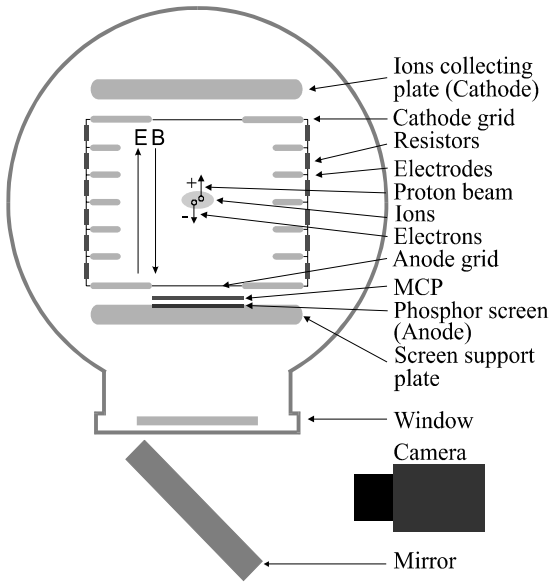

FIGURE 1. Schematic drawing of the Rest Gas Monitor..

The light, centred at λ=530 nm, is reflected by a 14 mm thick, Melles Griot 02MFG009 mirror, and hits a standard Fujinon CF25L, 1:0.85/25, TV lens. The distance from the phosphor screen to the lens input is 250 mm. The Vision VV5402 CMOS camera, is connected to control and acquisition electronics located in a VME crate at the surface, via a 200 m long multiple-wire cable. Data are sent to a distant computer using an ethernet transmission. A Graphical User Interface displays the acquired data on a X-terminal, in two different modes: every 40 ms during an acceleration cycle, a profile is integrated over 20 ms (866 SPS turns). The profiles can then be examined one by one or displayed in a mountain-range plot. The evolution of position, intensity or rms value is plotted as a function of time. In the other mode, the data are plotted as a 2-D picture of the beam, or as an artificial 3-D graph with the signal amplitude in the third dimension (z direction).

Two lines, spaced by 20 mm, deposited on the screen support, are used for calibration. By illuminating the phosphor screen with a diluted electron beam, setting B = 0 T and low grid voltages, these lines provide a direct reference to the acquisition system. With the chosen optics a resolution of 160 μm/pixel is obtained.

Dedicated electronics has been developed to control the various high voltages. Special attention is given to safety, since a MCP can easily be destroyed. A monitoring program,

with adjustable parameters, continuously checks the voltages and initiates a power-down procedure if a value runs out of range.

VOLTAGE SETTING OPTIMISATION

Special effort was invested to determine the best voltage settings. With the magnetic field contribution, moderate Anode grid (Ag) and Cathode grid (Cg) voltages can be used without image broadening. However, these values cannot be too low as the MCP has the

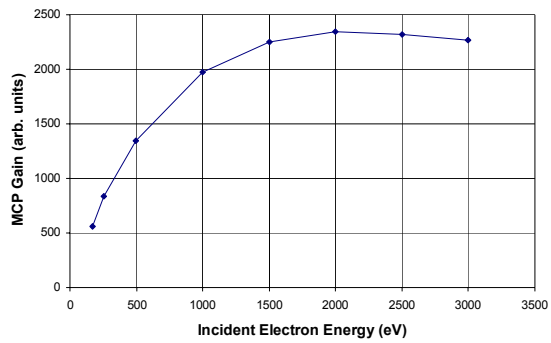

highest sensitivity for electrons with energies around 2 keV (Figure 2).

FIGURE 2. Measured MCP gain as a function of incident electron energy.

Primary electrons with too much energy cause secondary electron emission when they hit the grid wires. This effect adds to the desired distribution, as demonstrated in Figure 3 (left). On the contrary, if the grid voltages are too low, the wires mask a fraction of the primary electrons and a shadowing effect is observed, Figure 3 (right). Voltages between ± 1 kV and ± 2 kV on the grids seem to be the best compromise.

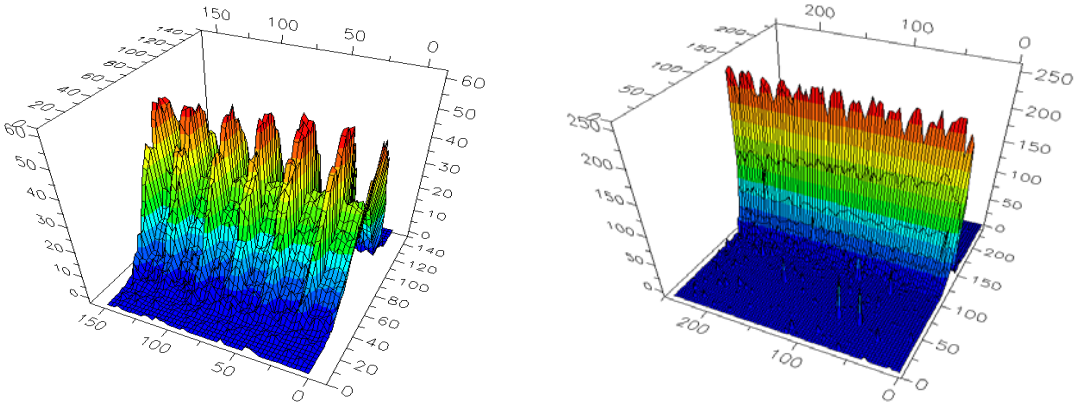

FIGURE 3. 3-D plots. Left: secondary electron emission. Right: grid wires masking effect.

The Cathode potential must be positive with respect to Cg to prevent the emission of secondary electrons produced by the impinging ions into the Cathode. These electrons would otherwise be attracted to the MCP and would disturb the signal of the primary electrons. The existence of secondary electron emission due to ions is illustrated in Figure 4.

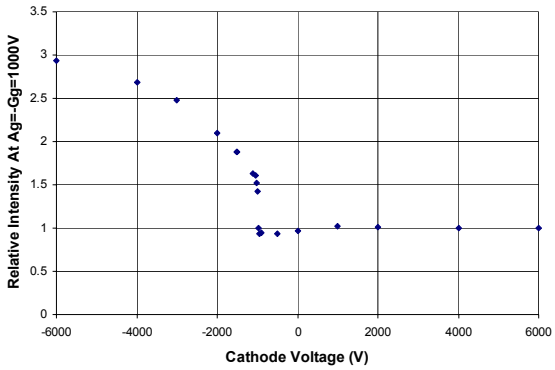

FIGURE 4. Signal intensity versus cathode plate voltage with Ag = - Cg = 1kV.

Setting Ag = - Cg = 1 kV and varying the cathode voltage from – 6 kV to 6 kV, the primary electron signal is affected as soon as the cathode voltage is lower than Cg. Towards more negative cathode voltages, ions have higher energy and their secondary emission yield on the cathode plate is enhanced. In practice, the cathode plate is left at ground potential and Cg always at a negative value.

The value of the MCP input voltage with respect to Ag is not critical. If too high, however, it enhances the secondary electron emission of the Ag wires. The differential voltage on the MCP controls its gain, with a maximum value of 1.2 kV.

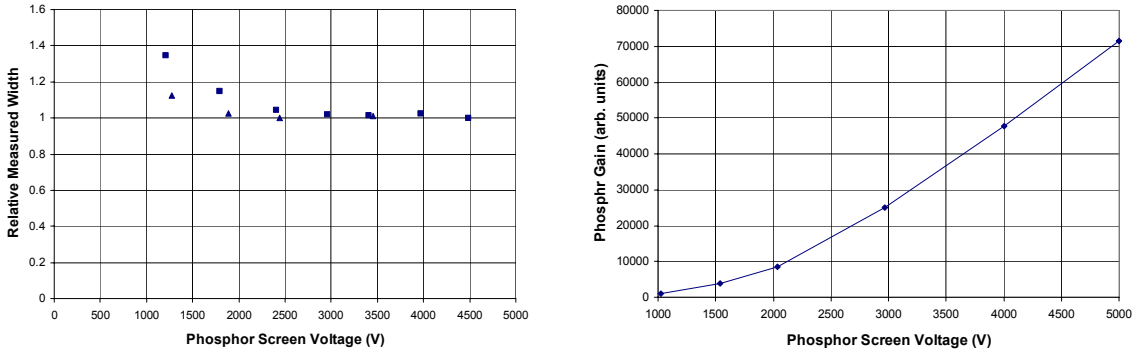

FIGURE 5 Relative measured beam width (left) and phosphor screen gain (right) as a function of the phosphor screen (anode) voltage.

Electrons leaving the MCP output face with low energy of a few eV, are accelerated onto the phosphor screen. Tests showed that the measured beam width decreases with increasing voltage, until 3 kV is applied, Figure 5 (left). In parallel, a regular increase of the phosphor screen emission is observed, Figure 5 (right). In the left plot, triangles and

squares represent two different fluxes of incident electrons. For low screen voltages, larger dimensions are measured at higher intensities (squares). The effect progressively vanishes with increasing voltages. A voltage of 3kV or more between MCP and screen is the best choice.

COLLECTED DATA

With improved understanding of the monitor behaviour and with optimised voltage parameters, data have been recorded under two different beam conditions. First, during SPS fixed target operation, when 4200 bunches of 5 10^9 protons are accelerated from 14 GeV to 450 GeV, and secondly during machine studies to prepare the LHC beam conditions, with 81 bunches of 3 to 4 10^{10} protons circulating at 25 ns intervals. Taking data with this LHC type beam is usually more problematic. Indeed, the anode grid voltage is very much affected, when the magnetic field is ON, by beam losses experienced throughout the acceleration cycle.

Adding extra shielding upstream the monitor did not solve this problem, which is still being investigated. Clearing electrodes and a loss monitor were installed during the winter stop for that purpose. In Figure 6, profiles are shown, recorded under either beam

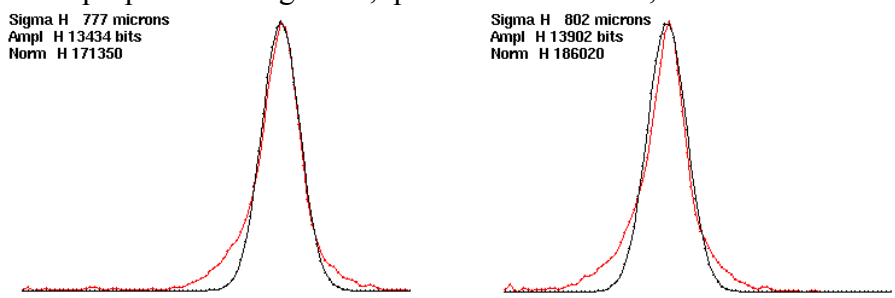

conditions at the end of the acceleration cycle, (450 GeV), with the magnetic field set at the maximum value (0.06 T). Both profiles are similar with rms value around 800 μm. With respect to a gaussian fit, asymmetric tails are observed. On the left-hand side of the curve the tail shows up at 30% of the maximum, compared to 20% on the other side.

FIGURE 6. Proton beam profiles recorded at 450 GeV; Left: 5.10^9 p/bunch – Right: 4. 10^{10} p/bunch.

Reproducibility, Precision, Resolution

During the acceleration of an LHC type beam, the energy of 450 GeV is reached at 12300 ms, followed by the beam extraction explaining the further shrinking of the beam dimensions.

Results of three consecutive acquisitions are summarised in Table 1.

Timing	Approx. beam energy	rms from gaussian fit 1	2	3	Average rms <σ>	Standard deviation s	Precision s/<σ>
(ms)	(GeV)	(μm)			(μm)	(μm)	(%)

7622	185	1246	1232	1250	1243	9.5	0.8
8702	280	1030	1027	1028	1028	1.5	0.1
9742	330	861	892	897	883	19.5	2.2
10942	400	797	794	793	795	2.1	0.3
12342	450	729	725	727	727	2.0	0.3
13902	450	674	663	664	667	6.1	0.9
14302	450	450	489	515	485	32.7	6.5

TABLE 1. Data of three consecutive acceleration cycles of an LHC type beam

The rms values result from a gaussian fit, ignoring the data below 30% of the maximum to overcome the effect of tails. This threshold was adopted after investigations, as it provided the best performance for the fit. Varying it between 10% and 50% leads to variations of ± 2% of the results. The reproducibility is such that a precision better than 1% is in general obtained on 3 consecutive cycles for rms values below 1 mm. This figure contains both the instrumental error and possible beam instabilities.

Effect of the Magnetic Field Strength

Profiles recorded at 450 GeV, when the magnetic field strength is varied from 20% to 100% of its full power, are shown in Figure 7. Figure 8 represents the evolution of the corresponding rms values, each value being averaged over data of four consecutive cycles. The precision is about 1%. Tails are not significantly affected by the magnetic field strength, except at low values where they are masked by the enlarged profile. However, increasing the magnetic field reduces progressively the rms value to an asymptotic value which is not completely reached at 100%, indicating that for measured rms values below 800 μm the resolution could be improved with a stronger magnetic field. This is in good agreement with predictions: an average broadening of 5% is expected, with B at 100%, for rms values of 800 μm due to the initial electron velocity distribution. In the case of the LHC type beam, this figure is increased to 6% with the additional contribution of the stronger beam induced electric field.

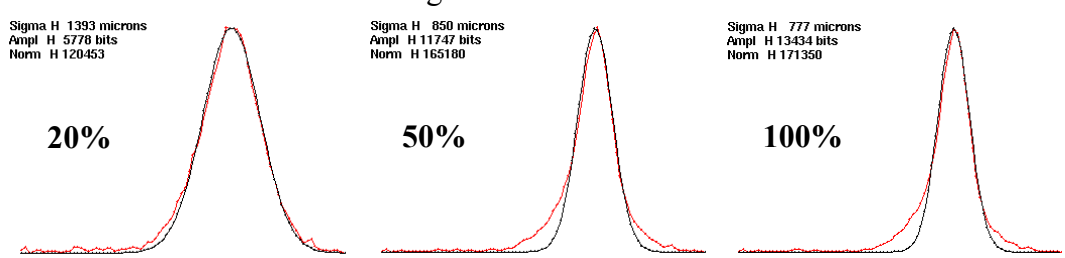

FIGURE 7. Profiles taken at 450 GeV with the magnetic field at 20%, 50% and 100% of maximum.

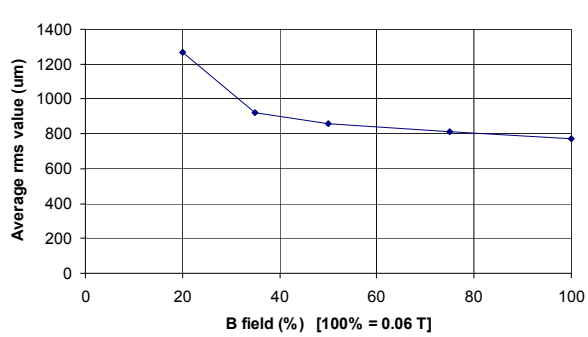

FIGURE 8. Rms value evolution with the magnetic field varying from 20% to 100% of maximum.

Comparison between Rest Gas Monitor and Wire Scanner

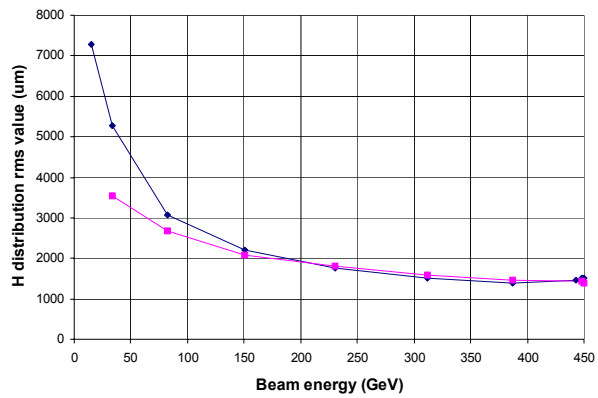

FIGURE 9. Parallel measurements made with the rest gas monitor (■) and a wire scanner (◆).

During acceleration to 450 GeV, the emittance contribution to the beam dimensions scales with $(E/ E_{inj})^{-0.5}$, E_{inj} being the injection energy and E the energy at which the measurement is taken. Data recorded with the rest gas monitor at different beam energies, are compared to the same data provided by a wire scanner, which is used as the reference for calibration of other devices. Results are presented in Figure 9. For this comparison, the rms values measured with the rest gas monitor are multiplied by 1.89, which is the theoretical machine optics ratio at the two monitor locations. For both devices, each measurement point is averaged over 4 acquisitions and the reproducibility is in the order of 1%. At the lowest energies of 34 GeV to 82 GeV, (first two common points), the rest gas monitor provides smaller values than the wire scanner. This difference is due to the contribution of dispersive effects to data measured by the wire scanner, where, contrary to the rest gas monitor location, the H dispersion is not zero. Above 100 GeV, the momentum dispersion becomes small and these effects vanish progressively. Both devices are then in agreement within 3% to 5%. Hence, considering the scaling factor applied, the rest gas monitor discriminates rms variations well below 1 mm. The discrepancies are within the error contribution coming from the instruments (1% for each device), and from the accuracy on the machine optics data. During the winter shutdown, a wire scanner was installed close to the rest gas monitor. This will allow for more precise cross calibration, suppressing the uncertainty on the knowledge of the machine optics.

Observation of Tails

As already mentioned, tails are observed on the rest gas monitor data with respect to gaussian fits. The problem is overcome by choosing an appropriated fit criterion. Nevertheless it is desirable to understand their source. They do not appear on wire scanner

data. However the two instruments do not have exactly the same acquisition mode and they may react differently to given phenomena experienced for example by the beam. Whereas the wire scanner samples at each beam revolution, a rest gas monitor profile results from integration over 866 turns. Tails do not seem to be beam current density dependent and do not result from secondary electrons coming from the cathode plate, as explained previously, considering the operational voltage settings. Widening of the signal due to photo-ionisation is also discarded. Machine studies are foreseen this year to investigate possible causes related to the beam.

Inspection of the monitor during the last winter stop revealed that the mirror was damaged along two edges and apparently had been submitted to important mechanical stress. Stress will cause the mirror to deform and will introduce image distortion. Modifications to the mirror support were implemented, but it was not possible to verify since the last SPS start-up whether the problem was cured.

SUMMARY

During the year 1999, more experience was gained with the rest gas profile monitor installed in the SPS. Optimised voltage parameters were identified with good understanding of the device behaviour. A few problems still need clarification. One of them is the monitor sensitivity to proton losses experienced during the acceleration of LHC type beams. Clearing electrodes and a loss monitor have been added to help understanding and curing this phenomenon, which might disappear when the SPS machine will be better tuned to these new beam characteristics. Another issue, although it is coped with by proper fitting, is the presence of tails showing up at 1.5 σ of the gaussian distribution. So far, it was not possible to verify if the different measures taken during the last winter shutdown, (realignment, modification of the mirror supporting system, replacement of the MCP and of the phosphor screen), did solve the problem. If not, investigations will be pursued, necessitating dedicated machine studies.

Nevertheless, the quality of the collected data is encouraging. In particular, the resolution better than one millimetre, which is aimed at to operate the LHC below 2 TeV, looks within reach with this type of instrument. A mechanically optimised device will probably even have better performance than this adapted prototype. One improvement will come from an increased magnetic strength. A more compact design is then necessary for incorporation within a magnet with a smaller gap. A factor 3 to 4 can probably be gained on B, which in any case will be needed to cope with the stronger space charge forces of the LHC nominal beam.

Another advantage of a rest gas monitor is the abundant signal, provided under operational vacuum conditions (10^{-9} to 10^{-8} hPa). Considering also the high speed of the liberated electrons, drifting within a few nanoseconds onto the MCP, the device appears to be well suited for turn by turn studies. Later in the year, tests will be carried-out to check this ability of the instrument.

ACKNOWLEDGMENTS

The kind help of J.L. Arduini to control the magnetic field during our tests is gratefully acknowledged, as well as the support of J. Camas and M. Sillanoli for all the mechanical issues.

REFERENCES

1. Bosser, J. et al., LHC Beam Instrumentation Conceptual Design Report, LHC Project Report 370, CERN, February 2000.
2. Connolly, R. et al., A Protoype Ionization Profile Monitor for RHIC, Proceedings of PAC 1997, Vancouver, p 2152.
3. Wittenburg, K, Emittance Measurements in the Proton Accelerator in DESY, Emittance in Circular Accelerators, KEK 95-7, Sept. 1995.
4. Fischer, C., and Koopman, J., Ionisation Profile Monitor tests in the SPS, Proceedings of DIPAC 1999, Chester, UK, May 1999, pp 119-121 and CERN-SL-99-046 BI.